

Reflectometry with a scanning laser ophthalmoscope

Ann E. Elsner, Stephen A. Burns, George W. Hughes, and Robert H. Webb

We describe noninvasive techniques to optimize reflectometry measurements, particularly retinal densitometry, which measures the photopigment density difference. With these techniques unwanted scattered light is greatly reduced, and the retina is visualized during measurements. Thus results may be compared for each retinal location, and visible artifacts are minimized. The density difference measurements of the cone photopigment depend on the optical configuration of the apparatus. The cone photopigment density difference is greatest near the fovea and for most observers decreases rapidly with eccentricity. A research version for reflectometry and psychophysics of the scanning laser ophthalmoscope is described.

Key words: Reflectometry, densitometry, scanning laser ophthalmoscope, cone photopigment, imaging.

I. Introduction

A. Problems with Reflectometry for Clinical Use

Techniques that measure the light returning from the ocular fundus (reflectometry) have been used in many laboratories to assess visual function in normal observers and in patients with eye and metabolic diseases (for a partial review see Refs. 1–4). In theory modern reflectometry also could be an efficient way to obtain objective, quantitative, and clinically useful information about the structure and function of the eye from fundus reflectance measurements. In practice reflectometry results are scarce compared with other techniques that are in widespread clinical use, e.g., electroretinography. New reflectometry techniques^{5–13} may make reflectometry more clinically applicable. Reflectometry data concerning the bleaching and regeneration of photopigments are reported for comparatively few patient groups and laboratories^{13–32} and rarely with a large sample of patients despite more than 30 yr of scientific study. In addition many new techniques give a clearer picture of the interaction of light with ocular tissues,^{33–41} and these provide a clearer picture of what is needed for further study of pathology with reflectometry.

Two types of recent technical advance have made

reflectometry possible in clinical populations. One is the use of more sensitive detection systems,^{5–7,17,18,25,31} which allow better measurements from the very limited amount of light returning to the detector through the pupil of the eye. The other is the use of imaging of the fundus during measurements.^{5–7,17,18,25} This allows more precise control of the measurement area and the minimization of visible artifacts such as reflections. Media problems such as cataracts, vitreous strands, and floaters are apparent.

The problems with the techniques of reflectometry are summarized in Table I. Some of these are inherent in reflectometry, such as eye movements during testing and a low signal-to-noise ratio of the light returning from the eye to the detector. Others are relevant only in certain patient groups such as highly reflective retinal pathology. Many problems, such as scattered light from the lens of the eye or low contrast in longer wavelength images, can be minimized by improved equipment and technique. We describe the techniques in terms of optimizing reflectometry measurements for use with patients.

B. Reflectometry Techniques with the Scanning Laser Ophthalmoscope

We are using reflectometry with the scanning laser ophthalmoscope (SLO) to investigate disease and aging mechanisms.^{1,5,6,8–12} The SLO^{42–44} can be used for several reflectometry techniques^{1,5,7,11,12} as well as psychophysics.^{10,45,46} The SLO provides an image of the retina that is the basis of the reflectometry measurements. Results can then be compared with pathology as seen clinically. Monochromatic imag-

The authors are with the Eye Research Institute, 20 Staniford Street, Boston, Massachusetts 02114.

Received 19 September 1991.

0003-6935/92/193697-14\$05.00/0.

© 1992 Optical Society of America.

Table I. Potential Problems with Reflectometry

- (1) Changes in measurement site with
 - (a) eye movements
 - (b) head movements
- (2) Changes in the amount of light reaching the detector with
 - (a) eye movements, including pupil vignetting and angle of incidence of illumination and detection pathways
 - (b) blinks
- (3) Selection of the measurement site from
 - (a) visual fields or angiography
 - (b) pathological tissue with unknown reflectance properties
- (4) Scattered light from
 - (a) anterior segment—cornea, lens, lens capsule
 - (b) vitreous
 - (c) inner limiting membrane and nerve fiber layer
 - (d) highly reflective retinal pathology
- (5) Low signal-to-noise ratio from
 - (a) low reflectance of the tissues of interest
 - (b) the small sampling angle of the pupil of the eye
- (6) Low contrast or defocused images from
 - (a) poor contrast of longer wavelength stimuli
 - (b) focus at one wavelength, imaging at another
- (7) Lack of adequate models for
 - (a) distribution of pigments across the fundus
 - (b) scattering from and absorbing in eye structure
- (8) storage and processing of large amounts of data (at least 1/4 Mbytes/present image)

ing, fluorescein angiography, and other SLO views all provide different information about the same structure. In this paper we describe optimizing an SLO for reflectometry, some limitations of reflectometry, techniques to obtain the spatial distribution of the cone photopigments, using an SLO, and reflectometry results. The goal is to assess the health of the outer retina and retinal pigment epithelium, as well as the cones and their metabolic support, and to do this noninvasively, quickly, and objectively.

II. Method

The present SLO is similar to other confocal instruments with laser scanning.⁴²⁻⁴⁴ A laser beam scans the eye at video rates. The horizontal scanner is a rotating polygon; the vertical scanner is a galvanometer. Light returning from the eye travels back through the same scanners to a beam separator at a pupil conjugate plane on the source side of the scanners. The reflected light is diverted there to the detector pathway. This light forms an image in a plane conjugate to the retinal plane, where there are a series of apertures. The detector (following such an aperture) is in the plane of the pupil of the eye where the retinal image is defocused. The detector, which integrates the light at this pupil plane, is sampled at video rates. This produces the video-rate raster that is seen by the subject and an image of the eye that is seen by the experimenter. Because the illumination

beam is moved continuously, only one retinal location at a time is illuminated. The light returning to the detector is not spatially separated, as it would be in a CCD camera. Instead the light returning is separated temporally because only light returning when a given point is illuminated is coded as light from that point. Optical cross talk, which is unwanted light, is eliminated further in that the SLO is confocal; the series of apertures in a plane conjugate to the retina eliminate light scattered from objects that are outside the focal volume. Movable optics to compensate for the subject's refractive error can also be used to focus in different depth planes at the retina. This also allows compensation of the eye's and the instrument's chromatic defocus.

A. Apparatus

Recent technological advances in confocal imaging and electro-optics have led to the development of different types of imaging instruments, each suited for different purposes. The SLO that is described here (Fig. 1) has several advantages for reflectometry, which make it different from other laser scanning and reflectometry instruments.

1. Optics

Five light sources are combined by dichroic mirrors: a 633 nm He-Ne laser, an 830-nm diode laser, a 594-nm He-Ne laser, a 543-nm He-Ne laser, and a multiline (514, 488, . . . nm) Ar-ion laser. External neutral-density wedges and filters control the irradiance of each laser. Interference filters select the

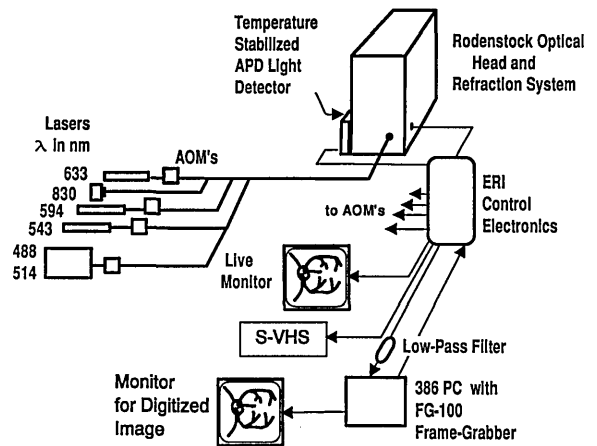


Fig. 1. Schematic diagram of the SLO that is used in these experiments. Light from five lasers is combined by dichroic mirrors: a 633-nm He-Ne laser, a 830-nm diode laser, a 594-nm He-Ne laser, a 543-nm He-Ne laser, and a multiline (514, 488, . . . nm) Ar-ion laser. Neutral density wedges and filters control the irradiance. AOM's provide graphics and blanking of the retrace lines independently for all four visible wavelength lasers. The combined light passes through the circular port of the beam separator of the Rodenstock optical head. The Eye Research Institute custom-built electronics include circuits for motor control of the Rodenstock scanning and focus compensation system, cooling of the avalanche photodiode detector (APD), and the generation of video synchronization. They also amplify and condition the video signal for data collection.

wavelength of the Ar laser. The maximum available power at the cornea from each laser is at least $100 \mu\text{W}$ for all lasers except the 543-nm He-Ne lasers, which is only $40 \mu\text{W}$. An acousto-optic modulator (AOM)⁴⁷ is placed in the beam path of each of the four visible wavelength lasers. These AOM's modulate the intensity of each beam to provide graphics and blanking of retrace lines. The attenuation is controlled either by computer or manually for precise control of beam power. All laser beams pass through the circular port of the beam separator on input. This aperture is at a plane that is nearly conjugate to the eye's pupil. Since the aperture is of fixed size and the laser beams are generally collimated here, both the size and focal plane of the raster and image are similar across wavelengths.

From this beam separator to the eye, and then to the detector, the optics are the new refraction and scanning system from Rodenstock Instruments (Rodenstock 101).⁴³ Detection apertures are mounted on a rotatable wheel for ease of changing.

2. Electronics and Computer Interface

The electronic and computer control of the SLO is customized to allow quantitative calibration or adjustment of the following: the control voltage applied to each AOM, the focusing optics, the height of the raster, the detection aperture selector, and the detector bias voltage. All these operate independently from image acquisition. The detection aperture selector and the lens components of the focusing optics are controlled by an IBM compatible computer and stepper motors.

The detector, an APD,^{42,48} is held at a constant temperature for greater stability. For silicon the quantum efficiency, and therefore the signal-to-noise ratio, increases with wavelength in the range of wavelengths used. Thus a Si detector is a good choice for cone photopigment measurements and infrared imaging. In addition this detector has an advantage over the photomultiplier tube for the practical reason that it is not readily damaged during accidental exposure to bright light. We use an RCA 30950E,⁴⁸ which is a hybrid unit containing an APD, an amplifier, and a temperature-measuring diode in its case. Our units are modified by the manufacturer (Spec. 710) for approximately twice the amplifier gain and a bandwidth of 25 MHz, which is half of their standard.

a. Video chain

The video chain is schematized in Fig. 2. It has been designed to be stable, to represent small changes over several minutes accurately, and to prevent corruption of the video signal or synchronization by bright or dark regions of the image (high or low voltages). We amplify a voltage representation of the reflectance variations that are encountered by the moving illumination beam, place it on a voltage pedestal, combine it with synchronization waveforms (the synch signal), and finally distribute it as composite video to low-

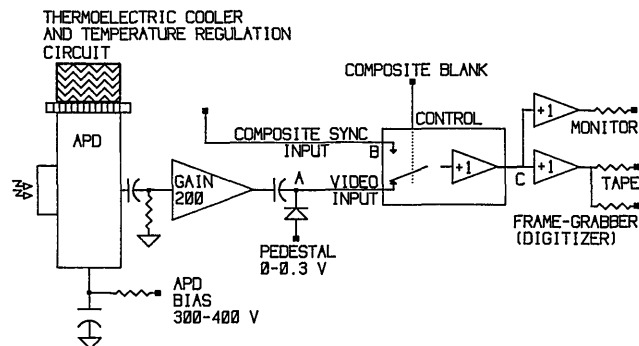


Fig. 2. SLO video system. The APD output signal is placed on a pedestal (A) and combined with the composite synch (B) to produce a composite video (C). The maximum system gain at a 600-nm incident light wavelength is $\sim 200 \text{ mV/nW}$ at C. The gain is controlled over a useful range of 10:1 by varying the APD bias voltage. See Subsection II.A.2.a for a discussion of composite synch generation. To stabilize the gain of the APD, its case is held at 10°C (50°F) by a thermoelectric cooler.

impedance monitoring, storage, or processing devices. The purpose of the pedestal is to restore a base-line or black level to the ac-coupled video signal.

The SLO composite video waveform is shown in Fig. 3 for a single horizontal line of video. The timing information for the entire system is contained in the synch signal, which itself is derived from the spinning 25-facet polygon that is used to produce the horizontal raster scan. A small infrared emitter/detector placed near the polygon determines the instant at which a scan begins, producing a horizontal synch pulse. These pulses are counted to create vertical beam deflection and synchronization information. This dependence of video signal synchronization on a mechanical (rotating) device is one of the distinguishing features of the SLO system and must be taken into consideration when attaching ancillary

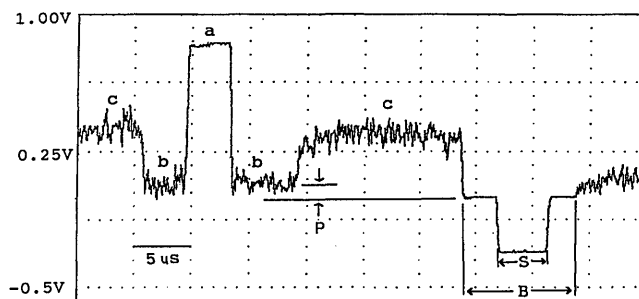


Fig. 3. Composite video output from the SLO during part of a horizontal scan line that is approximately in the middle of the raster. The target was made by putting a thin, vertical strip of white paper across a hole cut in matte gray paper (Ce oxide). The beam scan begins on gray (c), then encounters black (b) (the hole), white (a), and again black (b), and finishes on gray (c). The light level is adjusted so that there is saturation of the video signal at the white stripes. The detector bias voltage is set as in a retinal densitometry experiment. Data were collected with a logic analyzer (HP 1631D) using 50-ns samples. The signal is 0 V during the horizontal blanking interval B, except when it is interrupted by the negative horizontal synch pulse S. An adjustment raises the base line b to a pedestal level P of $\sim 5\%$ of the saturation.

video equipment. A minor difference from the National Television Standards Committee (NTSC) synchronization standard is the absence of serrating and equalizing pulses, which have been added on occasion by processing with a time base corrector. Otherwise, for the acquisition or presentation of images, the computer boards for graphics and data acquisition must synchronize with the SLO.

Composite video from separate channels is fed to three devices: an analog monitor, a computer board for both imaging and graphics (Imaging Technology FG100AT in a 386-based computer), and the luminance input to an S-VHS tape recorder. A separate signal with synchronization only is fed to the imaging board, since synchronization could be lost when the video signal is too large and corrupts the synchronization signal. As can be seen in Fig. 3 this is usually not the case. At the composite video signal prior to input to the computer there is a low-pass, antialiasing filter (TTE Inc. LVD945-3.60M-75-720B). This filter has a sharp cutoff at 5 MHz.

b. Raster graphics

The SLO has several advantages for experiments with visual stimuli. While the experimental method and data^{10,45,46} are better described elsewhere, this complete description of the current apparatus includes the generation of spatial patterns such as graphics. To produce graphics in the raster the AOM is driven by a computer graphics board in exact synchronization with the SLO at a 30-Hz frame rate (60-Hz field rate). This rise/fall time (trough to peak) of each AOM is generally the duration of a pixel (100 ns). The faster AOM function used for graphics pattern generation drives the device to its calibrated minimum, which may be 10^{-3} times the maximum light but not zero. Our graphics are controlled with the same computer as image acquisition, which is independent of all instrument control. There are 8 bits of pixel intensity available plus overlay planes. The raster is 512×480 pixels, although the outside edges of the raster are turned off on the SLO (see the discussion of uniformity below).

The SLO raster differs from familiar video display rasters in that there is no persistence or temporal averaging. Thus the duration of the light falling on each retinal location is very brief. In each field there are ~ 17 ms between the end of the illumination in the upper portion and the beginning of the illumination in the lower portion.

c. Image acquisition

The overall layout is shown in Fig. 1. The imaging board digitizes input to 256 levels of gray (8 bits of image gray level) and stores a video frame. We acquire images while viewing a monitor that presents what has been digitized and stored on the computer. During data storage there is no real-time representation on the acquisition monitor of the image of the retina. The live monitor allows continuous viewing of the unfiltered input. Up to four 512×480 -pixel

images may be taken in sequence at a 30-Hz frame rate before storage to disk. The images that are acquired by the computer include pixels outside the edges of the raster, which may be used for calibration.

3. Calibration

We aligned and calibrated with a model eye (Fig. 4) and a choice of targets in the retinal plane: a uniform reflector (MgO, Kodak white, 6080), diffusers to align the detection apertures, or 1-mm grid graph paper. Calibration of the image gray level and uniformity as well as absolute reflectance is done with the model eye and the uniform target. We use this target also to eliminate scattered light. We set the 633-nm laser to full power, protect the detector from light, and align with the light reaching the apertures, which is visible on a white surface in these conditions. Scattered light that does not originate from an image of the model eye is baffled. For further alignment of the detection apertures, we use a selection of diffusing papers and ground glass in front of patterned targets. We view them with selected detection apertures and then rotate the aperture selector under computer control to position the light on the aperture. We use the grid target for alignment and the size calibration of the image and raster. Raster size, shape, and uniformity as well as image uniformity require both electronic and optical adjustments. The size of the raster and the imaged area is chosen to be a 28.6×23.0 deg (large field) or 15.2×13.6 deg (small field) visual angle. The large field size is larger than that of previous confocal SLO's, which is an advantage for testing the peripheral retina. This also allows more vessels or fundus features to be included in the image during alignment. We adjusted the raster so that the vertical and horizontal pixel dimensions are identical in the raster: circles look round. The visual angle is computed by projecting a known pattern on the grid paper at a known distance from the nodal point. There are 3.5 or 1.9 arcmin/pixel for the large field and small field, respectively, which cover 0.59 or 0.18 cm² on a typical retina.

In our construction and alignment of this SLO we produced as spatially uniform a raster⁴⁹ and image as

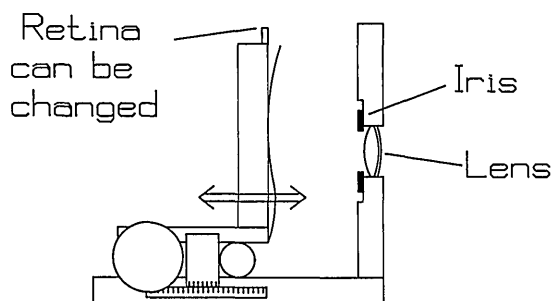


Fig. 4. Schematic diagram of the model eye. A sapphire lens (of 24.5-mm focal length) is centered in a 12-mm circular hole with an adjustable iris diaphragm. A selected retina is placed in a slide holder, which is adjustable in distance from the lens with a Vernier scale.

we could, even when that objective conflicts with others, such as maximizing raster size and intensity or minimizing the amount of light that is used to obtain an image. For example, the extremes, or edges, of a raster often exhibit many kinds of nonuniformity because of both system optics and the mechanical behavior of large, rotating mirrors. Our solution to this problem is to turn off (blank) the incoming laser beam by turning off the AOM at the raster edges completely. This process eliminates all except a small amount of scattered light from outside the (sharp) raster boundary and, equally important, eliminates flyback lines as the beam rapidly returns from right to left and from bottom to top. Turning off the AOM is somewhat slower electronically than the normal modulation (attenuation) system that can be used to impress graphic patterns on the raster, but it attenuates the light at least 3 log units more.

To calibrate the raster we measure the total power at the entrance pupil to the eye regardless of the portion of the field being calibrated, since the SLO is a Maxwellian view device. The intensity is uniform in the raster and the image. The measured intensity across the central 80% of the raster varies by $\sim 10\%$ (worst case). The SLO raster differs from most graphics monitor rasters in this uniformity. Monitor rasters lose intensity toward the outside edges.⁵⁰ In the SLO raster horizontal lines are perceived as separate, while video monitors blur this feature. Over time total laser power at the cornea (measured with an EG&G 2550 radiometer with the flat energy filter) varies little after the warm-up period (from $\sim 2\%$ for Ar and the 543- and 633-nm He-Ne laser and $\sim 5\%$ for the 594-nm He-Ne laser and the 830-nm diode). The image gray level varies over time by an amount that is similar to laser power, so that the variability seems not to be in the imaging pathway. Image uniformity is adjusted by using an oscilloscope as well as by quantifying the gray level in selected parts of digitized images by using a model eye. Image uniformity in experiments is highly dependent on the optics of the subject's eye.

4. Image Signal-to-Noise Ratio

We have investigated several standard ways of improving the signal-to-noise ratio in images. Spatial averaging within an image has been used for quantitative comparisons among conditions.^{5,6} Averaging successive images (temporal averaging) gives the expected square root of the sample size improvement for noisy images.⁶ In contrast in the data that we refer to here the noise is low enough that the digitized images show less than the square-root improvement.

Two images of a fixed target that included all levels of gray were taken several minutes apart, then averaged (gray level, 82.0 ± 55.1 , 82.2 ± 51.3). When subtracted, the resulting gray level is minimal (2.5 ± 2.6 for a 512×480 -pixel image; pixel values of less than zero are set to zero). This is reflected as an uncertainty in density difference measurements as 0.03.

We do not try to improve the perceived contrast in the image by increasing light levels or the detector bias voltage. Most reflectometry experiments are performed at a fixed gain and light level (which are chosen from pilot studies) to permit quantitative comparisons across time or wavelength.

III. Reflectometry Studies: Distribution of Cone Photopigment Optical Density

A. Optimizing the Reflectometry Technique

Retinal densitometry is a reflectometry technique that measures the amount of photopigment in the retina. The cone photopigment amount is described as optical density, which is the logarithm of the amount of light absorbed. Optical density usually refers to a transmission measure. Retinal densitometry measures the ratio of the amounts of light reflected between two conditions or locations; this quantity is expressed as a density difference. This quantity is proportional to the volume of photopigment across the retinal surface that is available to absorb photons of the appropriate wavelength. Important factors are photoreceptor coverage (the percent of retinal area that is covered by cones), light lost between cones, the photopigment extinction spectra, path length (including photoreceptor orientation), and photopigment concentration within a cone. We assume that only the photopigment that is unbleached can absorb light. Cones that are not oriented along the optical path will have a lower density difference.¹⁴ Photoreceptors that do not have a functioning neural pathway may still absorb light.

The distribution of cone photopigment changes as the unbleached photopigment is bleached. We measure the ratio of amounts of light returning from a given retinal area. First, the eye is dark-adapted to allow as much photopigment as possible to regenerate. Next, the retina is illuminated, and the amount of light returning to a detector is recorded immediately. After exposure to light that is bright enough to bleach most of the photopigment (in the present paper this is the same as the measurement light), the amount of returning light is again recorded. It increases since the photoreceptors do not absorb as much. The density difference that is computed from the difference in the logarithms of the images is 0.2–0.45 log unit in the fovea,^{5–10} depending on wavelength and the apparatus configuration. The density difference measurement includes all light returning to the detector, whether it passes through the cones once (going in), twice (going both in and out), or not at all (reflected or scattered back from structures other than the cones). Retinal densitometry can be confounded by scattered light returning to the detector. If there is light returning to the detector from structures that do not change with bleaching, the density difference is lower. Light returning from between normal photoreceptors, from between missing photoreceptors, from misaligned photoreceptors, from photoreceptors with a decreased concentration of photopigment, and from similar sources tell us

about the health of the outer retina. For example, disruption of the photoreceptor waveguide or the presence of extensive edema would decrease the measured density difference. For these reasons it is important to remove all known sources of unwanted scattered light. Traditionally these have been thought to be from the anterior segment and vitreous (see, for example, Ref. 26). The SLO discriminates well against these, but layers near the plane of focus are visible in certain circumstances.

In reflectometry it is important to obtain a high density difference, since then we can use the parameters producing this condition in techniques with patients. We must be confident that changes in the density difference reflect the pathologies being studied rather than artifact. For a high density difference measurement it is important to maximize the capture of the light returning from the deeper retinal layers, which contain the photopigment, and minimize light from other sources. Sampling the light returning from various parts of the eye is possible with the SLO by varying the imaging aperture. In previous studies we explored this by varying the imaging mode: open confocal mode (1250- μm aperture in the retinal plane) or closed confocal mode (200- μm aperture in the retinal plane) (Fig. 5).^{5,6} We found that the open confocal mode gives a larger photopigment density difference for the central 2 deg with 514-nm light. The open confocal mode samples relatively more light from the deeper layers, which contain the choroidal blood and melanin, the retinal pigment epithelium, macular pigments, and photopigments. The closed confocal mode samples light from the plane of focus, since the aperture limits the out-of-focus light. By selecting the imaging mode and illumination wavelength to optimize for a given measurement, blood vessel contrasts and optical densities of photopigment and macular pigment are as high as, or higher than, those found with other methods.

In this experiment we compared open confocal mode imaging with indirect mode imaging in which there is a central stop optically conjugate to the retina, which blocks light returning back at a narrow angle to the detector (Fig. 5). This decreases direct reflections from the fovea and foveal crest^{33,34,36} but also decreases the maximum possible density difference.³³

For cone density difference measurements we chose a monochromatic technique using 594 nm.³¹ Although cone photopigments absorb more light at 514 or 543 nm, and thus have higher densities, there is relatively little rod absorption at these wavelengths.⁵¹ Thus higher density differences are found with 514⁵⁻⁸ or 543 nm. However, reflection artifacts from the inner limiting membrane, the nerve fiber layer, and the foveal reflex are typical.³⁶ Also, the rod contribution must be eliminated by a multiwavelength method; then the density difference distribution is calculated by assuming (a) the spectral sensitivities of rods versus cones and (b) the spectral

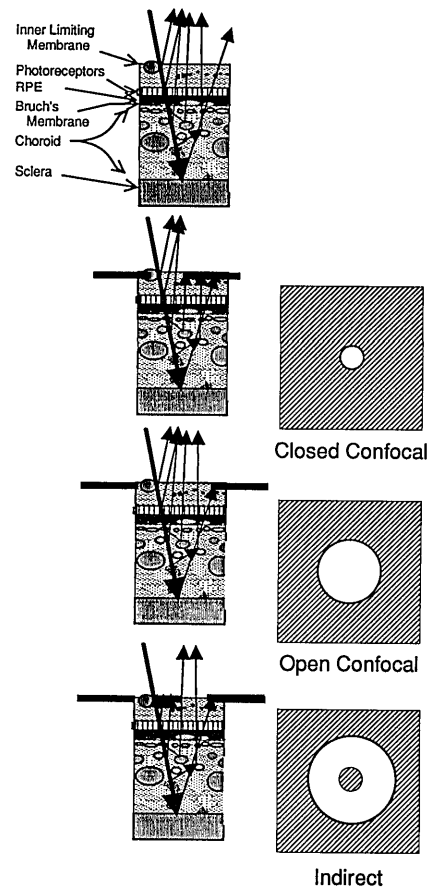


Fig 5. Schematic view of the apertures and imaging modes (see Ref. 5). The lateral spread of light scattered from the structures of the retina, choroid, and sclera is sampled differently by different apertures. The structures from the anterior segment and vitreous are not shown, but these layers above the retina would be blocked or passed by the selection of the aperture analogously to the retinal, choroidal, and scleral layers. (Top row) Imaging without an aperture. The light that is scattered from many layers of the ocular fundus may reach the detector. (Second row) Small confocal aperture. Only light from nearby structures and layers can pass through the aperture to reach the detector. (Third row) large confocal aperture. Light that is more widely scattered or from deeper layers may return to the detector. (Bottom row) indirect mode aperture with a circular stop blocking light from nearby structures and superficial layers of the retina. Only more widely scattered light or light from deeper layers can pass through the aperture.

differences in the reflectivity of the fundus.³³⁻³⁵ In particular, the measurement of the photopigment can sample light that is scattered from the superficial layers and also light that is scattered with a wider lateral distribution, which originates in the deeper layers. The latter component is thus strongly influenced by the absorption by choroidal blood and melanin,³⁵ for which there are individual differences. The larger spectral dependence that was observed previously in the open confocal mode corresponds to the spectral signatures of these choroidal pigments,⁵ conversely the spectral signatures of all pigments in layers surrounding the photopigment influence the light returning to the detector including light that is

returning to the detector from the deeper layers through the photopigment layers. Although there is less difference between the confocal and open confocal imaging mode at shorter wavelengths (514 nm) than at longer wavelengths, there is still high absorption of a short-wavelength light in the deeper layers. This decreases the lateral spread of the incident light, but the extent depends on the amount of choroidal blood and melanin. Thus the selection of the imaging mode and wavelength interacts, and multiwavelength techniques using shorter wavelengths must account for individual differences in these factors.

B. Reflectometry Method

For the comparison of apertures two male subjects were tested who were 26 and 55 yr of age. Only one aperture was used per experimental session with a rest period of at least several hours between session. Six other observers (five males with normal color vision who were 21, 25, 39, 40, and 50 yr of age, one female who is a carrier of anomalous trichromacy aged 50 yr) were tested with the indirect aperture. Two subjects (ages 26 and 50 yr) are known to have photoreceptors that do not point within 2 mm of the center of the pupil of the eye.⁴¹ Informed consent was obtained after the nature and possible consequences of the studies were fully explained.

The open confocal mode aperture was the largest circular aperture available that eliminates a visible corneal reflex; light returns to the detector from the central 800 μm of the retinal image plane. The indirect mode aperture was an annular aperture that blocked approximately the central 200 μm of the retinal image plane but permitted the more laterally scattered light to pass from a 1250- μm diameter in the retinal plane.

After pupil dilation the subject was dark-adapted for 15 min. Alignment to the instrument was performed with 830-nm light that was invisible to the subject. The plane of focus was determined from the sharpness of the largest retinal vessels, which were adjusted in the open confocal mode. The subject then viewed a bright (5.2-log Td) 594-nm light covering 28.6×23 deg. This retinal illuminance is sufficient to give the maximum difference in optical density in color matching experiments with an exposure of 2 min or less.⁵² Four images were digitized in 4/30 s at initial exposure; then additional images were digitized at ~ 1 -min intervals until no further pigment bleaching was observed.

1. Data Analysis

The density difference was calculated from an average of two or more selected images for both the dark-adapted condition (initial exposure) and the bleached condition (at least 2 min after exposure). Images were selected by viewing candidate images, then taking the logarithm of each. For the subtraction of images that were taken several minutes apart (dark adapted versus bleached) alignment of images

is necessary. The blood vessels served as registration landmarks for each image. We increased the field size from our previous work^{5,6} so that the bifurcation point of vessel branches provides a clear criterion for registration. One landmark was used unless there was substantial movement; then the average displacement from two or more was used. These landmarks are picked as near to the fovea as possible. It was rarely necessary to align the four successive images that were used in the average. We performed a translation calculation, since our imaging board has hardware pan and scroll capabilities. The logarithm of the dark-adapted image is digitally subtracted from the logarithm of the bleached image. A density map of cone photopigment is calculated for each pixel without spatial averaging. Darker indicates less density; lighter indicates more density. Features that appear black have no density, such as blood vessels, since there was a minimal change between the two images.⁵ Blood vessels not in alignment will appear as lighter than the background if they are from the dark-adapted image and darker if they are from the bleached image. Torsional movements are common, particularly from the reflexive eye movements following blinks. At the fovea where data are collected in this paper the displacement caused by rotation is minimal: 1 deg of rotation at 2 deg eccentricity (toward the outer edge of our data) is only ~ 0.6 pixel.

The position of the anatomical fovea is verified in two ways. First, there is a foveal reflex in the images, which is more visible in the direct mode. This is always represented in the data by a slight dip. Second, in subjects 1, 3, and 4 we compared the locations of fixation and the peak density difference. These differed by 1–2 pixels at most, which is within measurement error of the fixation locus.

2. Hard Copy

Images are converted to a tagged-image-file format, which may be viewed on the computer monitor. Commercially available software then allows the concatenation of images beyond the resolution of our previous composite image displays, which reduced the resolution before the hard copy could be made. Images, or composites of images, are then photographed with a Polaroid Digital Palette (CI 5000).

C. Results

1. Appearance of SLO Fundus Images

The appearance of SLO fundus images acquired in the open confocal mode⁵ and indirect mode is different (Figs. 6 and 7). We first note these differences; then we quantify them. Photographic prints accurately show neither the dynamic range nor the contrast in images. In the indirect mode images have good contrast for large retinal vessels but not many other superficial structures including the optic disk. In the open confocal mode the superficial layers have a higher contrast. Stronger reflections

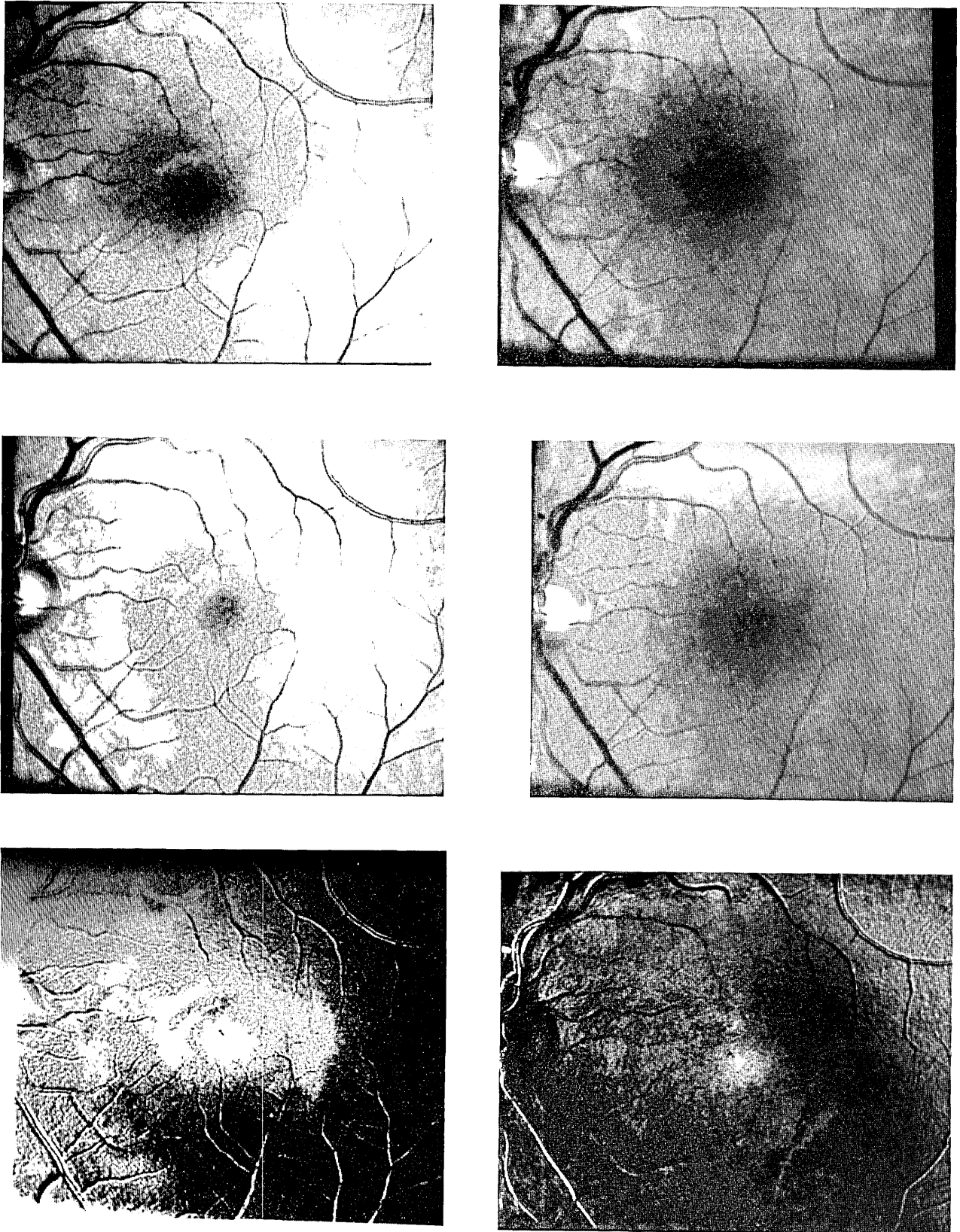


Fig. 6. Comparison of open confocal and indirect imaging in 594-nm light for a 26-yr-old male observer. (Top row) dark-adapted images; (center row) bleached images; (bottom row) distribution of cone photopigment density difference, which is obtained as a density difference from the dark-adapted and bleached images in the top and middle panels. Whiter indicates higher density difference; blacker indicates lower density difference. Left column, open confocal mode data; right column, indirect mode data. The photographic prints cannot reproduce the dynamic range and contrast in the images. The density difference in the lower left panel is shown in pseudo-color in Ref. 1.

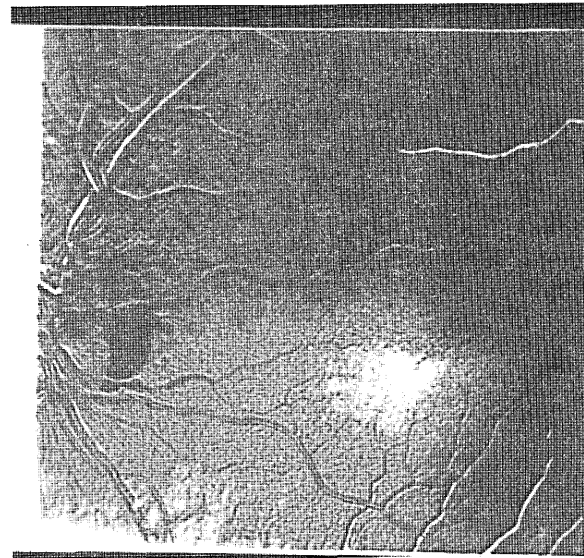
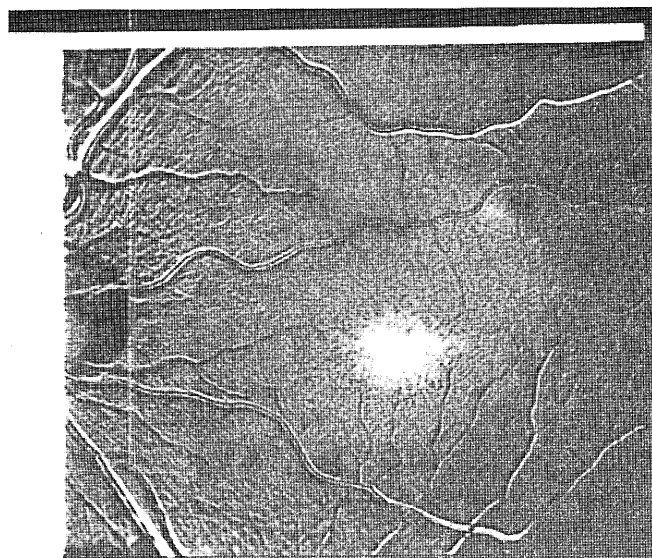
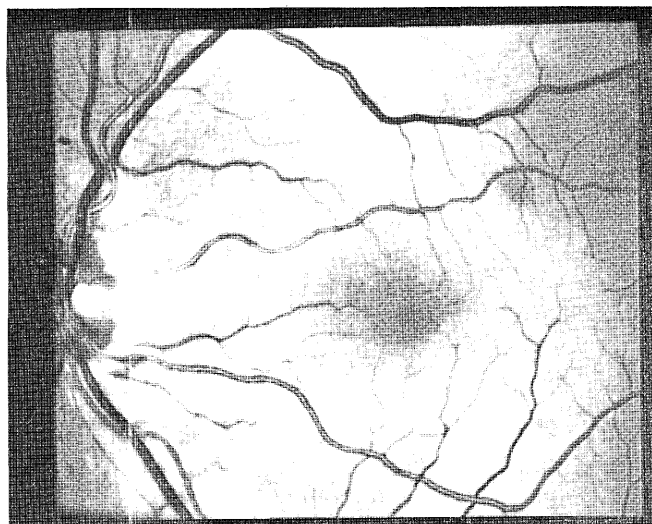
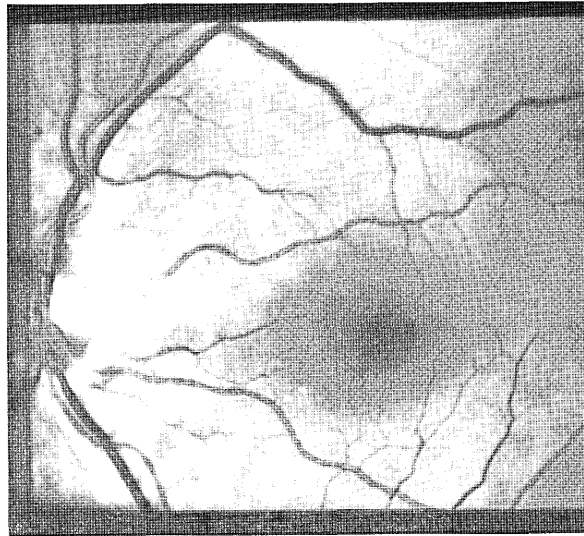
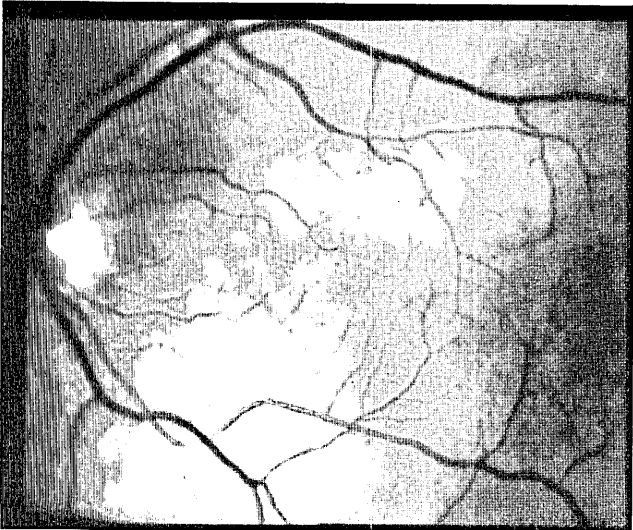


Fig. 7. Comparison of open confocal and indirect mode imaging in 594-nm light for a 55-yr-old male observer. The data are displayed as in Fig. 6. The large spot is the fovea; the smaller one is a floater, which moved during testing. The density difference in the lower left-hand panel is shown in pseudo-color in Ref. 1 along with the top and middle panels at the left.



(a)



(b)



(c)

Fig. 8. Images that are used in obtaining a photopigment density difference. They are acquired at 594 nm for a 21-yr-old male observer. (a) comparison of dark-adapted images (left) that were acquired with 594-nm light at 5.2 log Td with indirect mode imaging. (b) a bleached fundus image that is acquired in the same way. (c) distribution of the photopigment density difference that is obtained as a density difference from the dark-adapted and bleached images in the top panels. Lighter indicates high density; black indicates a density of zero. (Bottom right) control calculation of the density difference between two light-adapted images. This image more adequately represents the lack of density difference at peripheral locations and also the low contrast at the fovea in bleached images.

are seen in the younger observer at the foveal crest and from the nerve fiber layer in the open confocal mode. The foveal crest is somewhat apparent in the images of our youngest observer although minimized in this mode of imaging (Fig. 8). The foveal reflex is present but not prominent. Other than these features the images at 594 nm have a matte appearance, in contrast to many other wavelengths. One observer only has readily apparent choroidal vessels, which appear lighter than the surrounding area (Fig. 9). For our observers there is often better contrast of the small retinal vessels at wavelengths that are shorter than 594 nm or choroidal vessels at both longer and shorter wavelengths than 594 nm (not shown).

For 594-nm images in both imaging modes, the foveal area appears dark in the initial (dark-adapted) image and lighter after the bleaching of the photopigment. In Fig. 8 the reproduction of the bleached

image shows the foveal lightening best. The top and middle panels of Figs. 6 and 7 show the comparison of dark-adapted versus bleached images for both aperture modes, while the (a) and (b) panels of Fig. 8 and the top and middle panels of Fig. 9 show indirect mode imaging only. In previous results with 514-nm images the difference in the gray scale of the fovea between dark-adapted and bleached images is large (yielding a high density difference), but the difference is perceptually less noticeable in the raw image data for two reasons. First, at 514 (and 543) nm there is more absorption by macular pigments, which leaves a dark patch that is centered at the fovea in the light-adapted image. Second, there is a lightening of the rod-dominated retina that surrounds the fovea. Thus the whole 514-nm image becomes lighter with exposure to bright light; for 594 nm, which is selective for both long-wavelength cone photopigments, only the area inside the central 8 deg changes reliably.

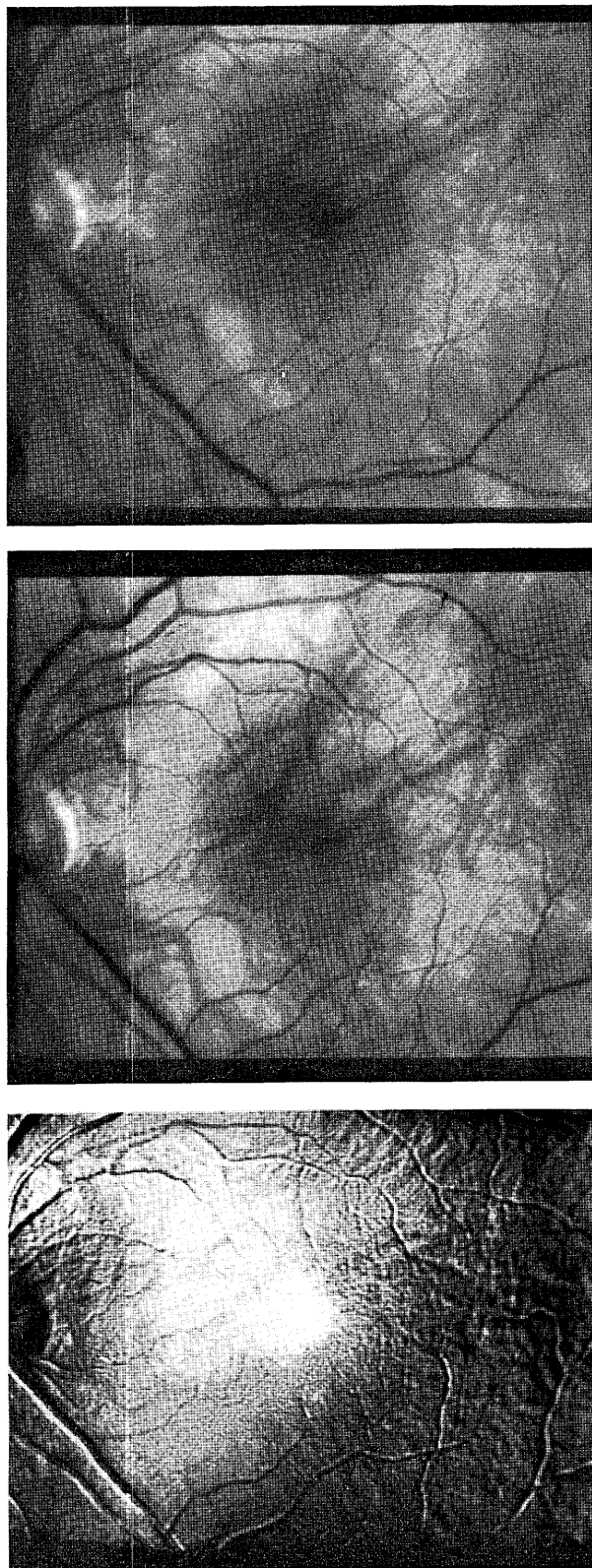


Fig. 9. Images that are used in obtaining the photopigment density difference for a 50-yr-old female observer. They are unusual in that the choroidal vessels are seen, yet a density difference is obtained. The data are displayed as in Fig. 8.

2. Cone Density Difference Measurements

The cone photopigment density difference, as measured by reflectometry, is highest in the central region and decreases with increasing retinal eccentricity. The images of the cone photopigment density difference distribution are shown (Figs. 5–9). The amount of density difference varies with the imaging mode. With the open confocal mode and the 10×10 -pixel sample near the center of the fovea, the density difference is 0.36 ± 0.040 for the younger observer and 0.25 ± 0.033 for the older observer. With indirect mode imaging the density differences are lower: 0.18 ± 0.030 for the younger observer (clearly lower) and 0.21 ± 0.031 for the older observer (which is not statistically different). Although more density is found for the younger observer with the open confocal mode, also more artifactual variation in the density difference is found, which is related to reflection artifacts (Fig. 6). For the worst reflection artifacts the apparent density differences are 0.28 and 0.098 in the open confocal mode and 0.098 and 0.11 for the indirect mode for the older and younger observers, respectively. No large or consistent nasal-temporal or inferior-superior differences are obvious in the images. The average differences are ~ 1 standard deviation less than the peak difference for each observer. A contour plot for subject 1 shows the density difference in graphic form. There is a clear artifactual decrease in the density difference near the foveal reflex (Fig. 11).

D. Discussion

Reflectometry measurements are potentially confounded by unwanted scattered light, which has many sources. The SLO minimizes scattered light since the illumination beam and detection pathways are synchronously moved, illuminating only one point at a time and detecting light from one illumination point at a time. In past studies one major concern has been to eliminate artifacts from light returning from the anterior segment, such as reflections from the cornea, lens, and vitreous. These artifacts are reduced in the SLO, which minimizes the light reflecting directly back from the cornea, lens, and other structures in the anterior segment of the eye. The part of this unwanted light that remains in the image is further minimized by the choice of aperture. An open confocal aperture minimizes the scattered light from other planes of focus. An indirect aperture still passes through some light from the anterior segment of the eye, but this light can be minimized by positioning the subject carefully. The indirect aperture minimizes light reflecting back from focal planes near the photoreceptors, which include such highly reflective surfaces as the inner limiting membrane and nerve fiber layer and the foveal reflex in normal subjects. In patients there is the possibility of reflections from the refractive-index differences at adhesions of the

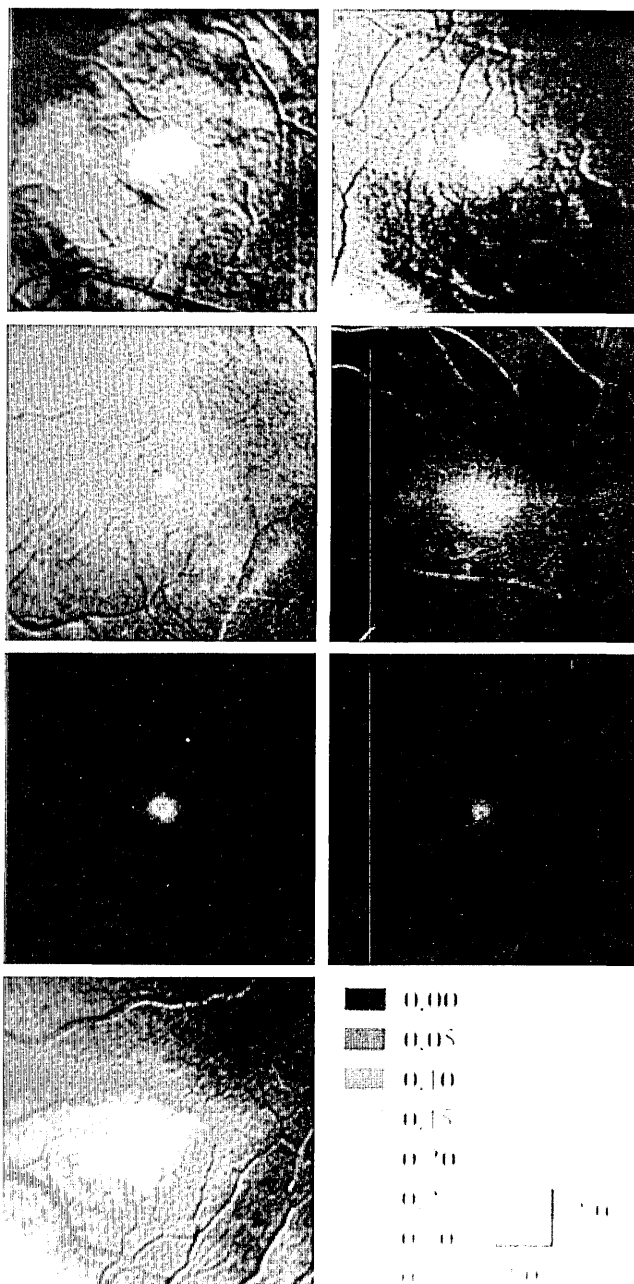


Fig. 10. Cone photopigment density distribution in the central 15 deg for the seven male observers in order of increasing age in years: top row, left (21) and right (25); second row, left (26) and right (39), third row, left (40) and right (50); fourth row, left (55) and right the density scale. All data were collected in indirect mode with the large field size. Lighter indicates a higher density difference; darker indicates a lower density difference.

vitreo-retinal interface, retinal scars, edematous tissues, and subretinal deposits, all of which are in the layers near the photoreceptors. Thus, although using this technique (594 nm, an indirect aperture) gives a density difference that is less than the theoretical maximum, it is high enough to quantify whether the cone photopigment is within normal limits and is less affected by artifacts that are regularly encountered in clinical populations.

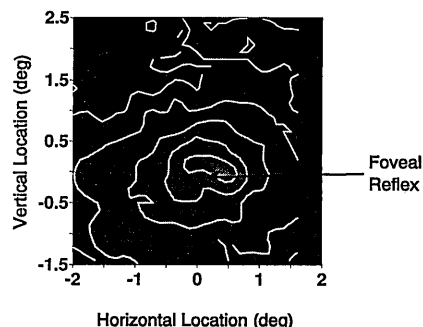


Fig. 11. Contour plot of cone photopigment density distribution for subject 1 superimposed on a smooth gray scale image. Density increments are 0.05. The highest density difference enclosed within a contour is 0.25, although the peak density is higher within this region.

The distribution of the cone photopigment density difference at 594 nm does not show measurable density that is indistinguishable from an artifact that is beyond ~ 3 deg (Figs. 6–9, bottom; Fig. 10 for most subjects; Fig. 11). In previous studies retinal areas that are more peripheral to the fovea were measured by using short-wavelength or multispectral techniques^{5–8} that can include rod optical density as well (for example, Refs. 18, 20, 25). However, these require more assumptions (see Section III.B), suffer from reflection artifacts, and require more data collection, storage, and processing. Thus, for studies in which foveal cone pigment optical density is of interest, as in studies of aging or disease that affect the retinal pigment epithelium, a single-wavelength technique is better.

The cone photopigment density distribution is similar in shape to the anatomical description of the areal coverage of cones across the human retina.⁵³ There is a maximum of cone coverage, and thus photopigment density difference, in the fovea and a decrease with eccentricity. There are so few rods in most subjects that measurement by reflectometry of the central 2 deg is infeasible, particularly with 594 nm. The low density differences that we find for cone photopigments at more than ~ 5 deg eccentricity correspond well with the rapid decrease in cone coverage. We find individual differences in the steepness of the decrease (Fig. 10). While individual differences are found for cone coverage, these are usually confined to the central 1 deg. Large individual differences have been reported previously when both rod and cones were measured.³² The source of our individual differences is left for a future paper.

Photopigment measurements are highly dependent on wavelength and technique as well as on the observer. As expected our density differences for 594 nm are lower than reported previously by using an SLO and 514 nm by us^{5,6} or van Norren and van Norren and van de Krats,⁷ since there is less optical density at this wavelength for normal observers. They compare favorably with measurements that were made with other techniques and wavelengths. Recent measurements made with reflectometers that

do not incorporate laser scanning include 0.084–0.317 at the maximum spectral sensitivity,³² an average of 0.32 at 554 nm,³⁰ 0.3 at 560 nm,²⁷ and 0.2 at 589 nm, which is referred to the infrared.³¹

Our technique addresses many of the problems of reflectometry as described in Section I.B. There is a sensitive but stable detector. There is typically no saturation of the detector following a large signal, such as from a blink, the optic disk, or a highly reflective scar (electronics example in Fig. 3). Visualization of the retinal position during measurement^{1,5–9,17,18,25} helps to minimize artifacts during testing. For example, the artifact in Fig. 7 was identified as a floater during testing, and images were digitized only when the position was away from the fovea. These provide at least partial solutions to limitations that are inherent in reflectometry concerning eye and head movements with respect to either the instrument or the detector. However, despite head stabilization, patients often do not have stable fixation, even if a fixation target is present, and images must be aligned. Even in normally sighted observers fixation is rarely stable enough to avoid the registration of images.

It is equally important that there is also improvement in reducing scattered light and improving the sampling of the light returning from the photoreceptor layer by the use of sampling apertures and scanning. There is good contrast at all wavelengths including long wavelengths that often have poor contrast in the fundus camera-based systems,⁵ and all wavelengths are in focus. Although we have not developed a new model of fundus reflectometry we use a technique that requires as few assumptions as possible. The processing of large amounts of data, currently one quarter of a megabyte per image, is simpler and quicker with a single-wavelength technique. From these and other experiments^{5,11,12} we are now beginning to understand more of the scattering/absorbing properties of the ocular fundus by reflectometry with different illumination wavelengths and imaging modes and may incorporate these findings in new techniques. For the present and possible future techniques the use of commercial software for personal computers eliminates some of the time-consuming and tedious steps in data analysis, making clinical reflectometry feasible.

These reflectometry techniques have been developed to examine visual function in patients with pathology that makes testing with previous methods difficult, such as patients with retinal detachment, media opacities, loss of central visual acuity, or poor fixation.

This work was supported by National Institutes of Health–National Eye Institute grants EYO7624 and DE-FG02-91ER61229. We thank Rodenstock Instruments for assistance with the optical head. We also thank A. Plesch and U. Klingbeil for stimulating discussions and T. Clune, R. Rappl, R. Schwarz, F. Rogomentic, and M. Kreitz for technical help. We thank the Polaroid Corporation for the use of the Polaroid Digital Palette CI5000.

References

1. A. E. Elsner, A. H. Jalkh, and J. J. Weiter, "New devices for retinal imaging and function evaluation," in *Practical Atlas of Retinal Disease and Therapy*, W. Freeman, ed. (Raven, New York, to be published).
2. J. E. Nasemann and R. O. W. Burk, eds., *Laser Scanning Ophthalmoscopy and Tomography* (Quintessenz-Verlag, Berlin, 1990).
3. J. E. E. Keunan, "Densitometry in diseases and senescence of the human retina," dissertation (State University of Utrecht, Utrecht, 1988) is an anthology of published articles and work in progress at the time. It is available from the author.
4. A. E. Elsner, ed., *Laser Scanning Ophthalmoscopy, Tomography, and Microscopy* (Plenum, New York, to be published).
5. A. E. Elsner, S. A. Burns, F. C. Delori, and R. H. Webb, "Quantitative reflectometry with the SLO," in *Laser Scanning Ophthalmoscopy and Tomography*, J. E. Nasemann and R. O. W. Burk, eds. (Quintessenz-Verlag, Berlin, 1990), pp. 109–121.
6. A. E. Elsner, S. A. Burns, and R. H. Webb, "Photopigment densitometry with a scanning laser ophthalmoscope," in *1988 Annual Meeting*, Vol. II of 1988 OSA Technical Digest Series (Optical Society of America, Washington, D.C., 1988), paper WY3. These first results (also Ref. 5) were for rod and cone photopigments and different instrumentation and technique.
7. D. van Norren, "Towards improved instrumentation for retinal densitometry," in *Research in Retinitis Pigmentosa*, E. Zrenner, H. Krastel, and H.-H. Boebel, eds. (Pergamon, Oxford, 1987), Vol. 62, pp. 177–178; D. van Norren and J. van de Kraats, "Imaging retinal densitometry with a confocal scanning laser ophthalmoscope," *Vision Res.* **29**, 1825–1830 (1989).
8. A. E. Elsner, S. A. Burns, and R. H. Webb, "Photopigment concentration in normal and photocoagulated retina." *Invest. Ophthalmol. Vis. Sci. Suppl.* **30**, 370. (1989).
9. A. E. Elsner, S. A. Burns, G. W. Hughes, and R. H. Webb, "Evaluating the photoreceptor/RPE complex with and SLO," in *Noninvasive Assessment of the Visual System*, Vol. 3 of 1990 OSA Technical Digest Series (Optical Society of America, Washington, D.C., 1990), pp. 40–43.
10. A. E. Elsner, S. A. Burns, M. R. Kreitz, and R. H. Webb, "Sensitivity maps vs. cone pigment density distribution," *Invest. Ophthalmol. Vis. Sci.* **31/4**, 108. (1990).
11. A. E. Elsner, R. Schwarz, S. A. Burns, and M. R. Kreitz, "Retinal light scattering," in *1990 Annual Meeting*; Vol. 15 of 1990 OSA Technical Digest Series (Optical Society of America, Washington, D.C., 1990), paper MD5.
12. A. E. Elsner, S. A. Burns, M. R. Kreitz, and J. J. Weiter, "New views of the retina/RPE complex: quantifying sub-retinal pathology," in *Noninvasive Assessment of the Visual System* Vol. 1 of 1991 OSA Technical Digest Series (Optical Society of America, Washington, D.C., 1991), pp. 150–153.
13. W. A. H. Rushton, "Kinetics of cone pigments measured objectively on the living human fovea," *Ann. N.Y. Acad. Sci.* **74**, 291–304 (1958).
14. H. Ripps and R. A. Weale, "Cone pigments in the normal human fovea," *Vision Res.* **3**, 531–543 (1963); "Photo-labile changes and the directional sensitivity of the human fovea," *J. Physiol.* **173**, 57–64 (1964); "Analysis of foveal densitometry," *Nature (London)* **205**, 52–56 (1965).
15. W. A. H. Rushton and G. H. Henry, "Bleaching and regeneration of cone pigments in man," *Vision Res.* **8**, 617–631 (1968).
16. M. Alpern, F. Maaseidvaag, and N. Ohba, "The kinetics of cone visual pigments in man," *Vision Res.* **11**, 539–549 (1971).
17. I. Fram, J. S. Read, B. H. McCormick, and G. A. Fishman, "In vivo study of the photolabile visual pigment utilizing the television ophthalmoscope image processor," in *Computers in Ophthalmology*, R. H. Greenfield and A. Colenbrander (Insti-

- tute of Electrical and Electronics Engineers, New York, 1979), pp. 133–144.
18. D. van Norren and J. van der Kraats, "A continuously recording retinal densitometer," *Vision Res.* **21**, 897–905 (1981).
 19. M. Alpern and D. H. Krantz, "Visual pigment kinetics in abnormalities of the uvea-retinal epithelium interface in man," *Invest. Ophthalmol. Vis. Sci.* **20**, 183–203 (1981).
 20. P. E. Kilbride, J. S. Read, G. A. Fishman, and M. Fishman, "Determination of human cone pigment density difference spectra in spatially resolved regions of the fovea," *Vision Res.* **23**, 1341–1350 (1983).
 21. V. C. Smith, J. Pokorny, and D. van Norren, "Densitometric measurement of human cone photopigment kinetics," *Vision Res.* **23**, 517–524 (1983).
 22. G. J. van Meel and D. van Norren, "Foveal densitometry in retinitis pigmentosa," *Invest. Ophthalmol. Vis. Sci.* **24**, 1123–1130 (1983).
 23. C. M. Kemp, D. J. Faulkner, and S. G. Jacobson, "Visual pigment levels in retinitis pigmentosa," *Trans. Ophthalmol. Soc. UK* **103**, 453–456 (1983).
 24. G. J. van Meel, V. C. Smith, J. Pokorny, and D. van Norren, "Foveal densitometry in central serous choroidopathy," *Am. J. Ophthalmol.* **98**, 359–368 (1984).
 25. D. J. Faulkner and C. M. Kemp, "Human rhodopsin measurement using a T.V.-based imaging fundus reflectometer," *Vision Res.* **24**, 221–231 (1984).
 26. P. E. Kilbride, M. Fishman, G. A. Fishman, and L. P. Hutman, "Foveal cone pigment density difference and reflectance in retinitis pigmentosa," *Arch. Ophthalmol.* **104**, 220–224 (1986).
 27. A. B. Fulton and R. M. Hansen, "The relationship of retinal sensitivity and rhodopsin in human infants," *Vision Res.* **27**, 697–704 (1987).
 28. A. B. Fulton and R. M. Hansen, "Foveal cone pigments and sensitivity in young patients with Usher's syndrome," *Am. J. Ophthalmol.* **103**, 150–160 (1987).
 29. L. T. Sharpe, D. van Norren, and K. Nordby, "Pigment regeneration, visual adaptation and spectral sensitivity in the achromat," *Clin. Vision Sci.* **3**, 9–17 (1988).
 30. D. van Norren and J. van de Kraats, "Retinal densitometer with the size of a fundus camera," *Vision Res.* **29**, 369–374 (1989).
 31. H. D. Baker, R. Henderson, and L. P. O'Keefe, "An improved retinal densitometer: design concepts and experimental applications," *Visual Neurosci.* **3**, 71–80 (1989). Although this paper uses 590 nm, there is also an infrared reference standard.
 32. P. E. Kilbride and K. M. Keehan, "Visual pigments in the human macula assessed by imaging fundus reflectometry," *Appl. Opt.* **29**, 1427–1435 (1990).
 33. D. van Norren and L. F. Tiemeijer, "Spectral reflectance of the human eye," *Vision Res.* **26**, 313–320 (1986).
 34. G. J. van Blokland, "Directionality and alignment of the foveal receptors, assessed with light scattered from the human fundus *in vivo*," *Vision Res.* **26**, 495–500 (1986).
 35. F. C. Delori, and K. P. Pfiibsen, "Spectral reflectance of the human ocular fundus," *Appl. Opt.* **28**, 1061–1077 (1989).
 36. R. W. Knighton, S. G. Jacobson, and M. I. Roman, "Specular reflection from the surface of the retina," in *Laser Surgery: Advanced Characterization, Therapeutics, and Systems*, K. Atsumi, N. R. Goldblatt, and S. N. Joffe, eds., Proc. Soc. Photo-Opt. Instrum. Eng. **1066**, 10–17 (1989).
 37. R. W. Knighton, S. G. Jacobson, and C. M. Kemp, "The spectral reflectance of the nerve fiber layer of the macaque retina," *Invest. Ophthalmol. Vis. Sci.* **30**, 2393–2402 (1989).
 38. J.-M. Gorrard, "Reflection characteristics of the human fovea assessed by reflecto-modulometry," *Ophthal. Physiol. Opt.* **9**, 53–60 (1989).
 39. J.-M. Gorrard and F. Bacin, "Use of reflecto-modulometry to study the optical quality of the inner retina," *Ophthal. Physiol. Opt.* **9**, 198–204 (1989).
 40. P. Artal, J. Santamaria, and J. Bescos, "Optical-digital procedure for the determination of white-light retinal images of a point test," *Opt. Eng.* **28**, 687–690 (1989).
 41. J.-M. Gorrard and F. C. Delori, "A method for assessing the photoreceptor directionality," *Invest. Ophthalmol. Vis. Sci.* **31/4**, 425 (1990); S. A. Burns, A. E. Elsner, J. M. Gorrard, and M. R. Kreitz, "Variability in color matching, photoreceptor alignment, and the Stiles-Crawford II effect," in *1991 Annual Meeting*, Vol. 17 of 1991 OSA Technical Digest Series (Optical Society of America, Washington, D.C., 1991), p. 24.
 42. R. W. Webb, G. W. Hughes, and F. C. Delori, "Confocal scanning laser ophthalmoscope," *Appl. Opt.* **26**, 1492–1499 (1987).
 43. A. Plesch and U. Klingbeil, "Optical characteristics of a scanning laser ophthalmoscope," in *New Methods in Microscopy and Low Light Imaging*, J. E. Wampler, ed., Proc. Soc. Photo-Opt. Instrum. Eng. **1161**, 390–398 (1989).
 44. A. Plesch, U. Klingbeil, W. Rapp, and C. Schroedel, "Scanning ophthalmic imaging," in *Laser Scanning Ophthalmoscopy and Tomography*, J. E. Nasemann and R. O. W. Burk, eds. (Quintessenz, Munich, Germany, 1990), pp. 109–121.
 45. A. E. Elsner, G. T. Timberlake, S. A. Burns, and M. R. Kreitz, "High illuminance perimetry: Photopigment Mechanisms," in *Noninvasive Assessment of the Visual System*, Vol. 7 of 1989 OSA Technical Digest Series (Optical Society of America, Washington, D.C., 1989), pp. 15–18.
 46. F. J. van de Velde, A. E. Jalkh, and A. E. Elsner, "Microperimetry with the scanning laser ophthalmoscope," in *Perimetry Update, 1990/1991*, R. P. Mills and A. Heijl, eds. (Kugler, Amsterdam, 1991), pp. 93–101; J.-F. Chen, P. L. Lou, A. E. Elsner, R. M. Hansen, H.-M. Cheng, and A. B. Fulton, "The effect of refractive error on retinal responses," *Invest. Ophthalmol. Vis. Sci.* **32**, 929 (1991).
 47. AEM-40 modulators with modified E40ER drivers, IntraAction Corporation, Bellwood, Ill. The AOM must be oriented horizontally, since the Fourier transform of the modulation pulse contains frequencies other than the carrier frequency and thus deflects the beam a little. The horizontal orientation assures that the deflection is equal in the scan direction.
 48. EG&G, RCA C30950E, Spec. 710 (Vaudreuil, Quebec, Canada).
 49. Scanned laser rasters do not have apparent speckle. S. A. Burns, M. R. Kreitz, and A. E. Elsner, "Apparatus note: a computer controlled, two color, laser-based optical stimulator for vision research," *Appl. Opt.* **30**, 2063–2065 (1991).
 50. W. B. Cowan and M. L. Rowell, "Phosphor constancy in color video monitors," *Color Res. Appl.* **11**, 34–38 (1986).
 51. G. Wyszecki and W. S. Stiles, *Color Science* (Wiley, New York, 1982).
 52. S. A. Burns and A. E. Elsner, "Color matching at high illuminances: the color match area effect and photopigment bleaching," *J. Opt. Soc. Am. A* **2**, 916–920 (1985).
 53. G. A. Osterberg, "Topography of the layer of rods and cones in the human retina," *Acta Ophthalmol.* **13** Suppl. 6, 1 (1935); C. A. Curcio, K. R. Sloan, Jr., O. Packer, A. E. Hendrickson, and R. E. Kalina, "Distribution of cones in human and monkey retina: individual variability and radial asymmetry," *Science* **236**, 579–582 (1987); C. A. Curcio, K. R. Sloan, R. E. Kalina, and A. E. Hendrickson, "Human photoreceptor topography," *J. Comput. Neurol.* **292**, 497–523 (1990).